Crystallization Kinetics and Mechanism of $CaO–Al_2O_3$-Based Mold Flux for Casting High-Aluminum TRIP Steels

CHENG-BIN SHI, MYUNG-DUK SEO, HUI WANG, JUNG-WOOK CHO, and SEON-HYO KIM

Non-isothermal crystallization of the newly developed lime-alumina-based mold fluxes was investigated using differential scanning calorimetry. The crystallization kinetic parameters were determined by Ozawa equation, the combined Avrami–Ozawa equation, and the differential isoconversional method of Friedman. It was found that Ozawa method failed to describe the non-isothermal crystallization behavior of the mold fluxes. The Avrami exponent determined by the combined Avrami–Ozawa equation indicates that the crystallization of cuspidine occurs through bulk nucleation and reaction-controlled three-dimensional growth, and then transforms to reaction-controlled two-dimensional growth at the crystallization later stage in lime-alumina-based mold fluxes with higher B_2O_3 content. For the mold fluxes with lower B_2O_3 content (10.8 mass pct), the crystallization of cuspidine is bulk nucleation and reaction-controlled two-dimensional growth at the crystallization primary stage followed by a diffusion-controlled two-dimensional growth process. The crystallization of CaF_2 in mold flux originates from bulk nucleation and diffusion-controlled three-dimensional growth, which then transforms to two-dimensional growth. FE-SEM observations support these kinetic analysis results. The effective activation energy for cuspidine crystallization in the mold flux with higher B_2O_3 and Na_2O contents increases as the crystallization progresses, and then decreases at the relative degree of crystallinity greater than 60 pct. The transition point of this trend approximately corresponds to the relative degree of crystallinity at which the crystallization mode of cuspidine transforms. For the mold fluxes with lower B_2O_3 and Na_2O contents, the effective activation energy for cuspidine formation varies monotonically with the increase in the relative degree of crystallinity.

DOI: 10.1007/s11663-014-0180-2

I. INTRODUCTION

CONTROLLING appropriate horizontal heat transfer and providing adequate lubrication during continuous casting process are the most important functions of mold flux.[1,2] Inappropriate horizontal heat transfer and lubrication performance of mold flux generally bring about serious operational problems in casting process (such as sticker breakout[1]) and various quality defects on cast slab, including severe oscillation marks, depressions, longitudinal cracks,[3–5] and so on. Many efforts have been made to study the heat transfer and lubrication performance of mold flux.[6–10] It has been generally accepted that the horizontal heat transfer between solidifying steel shell and mold is strongly dependent on the crystallization characteristics of mold flux.[1,7,11,12] Therefore, it is necessary to ascertain the crystallization behaviors of mold flux in the design of mold flux for meeting the requirement of both heat transfer and lubrication performance in continuous casting process.[2] The crystallization kinetic analysis is believed to be an effective method to reveal the mold flux crystallization mechanism and the differences in the crystallization ability of various mold flux systems. Therefore, a crystallization kinetic analysis would provide a guide for designing mold fluxes and optimizing the crystallization of mold fluxes.

Although the crystallization behaviors of various mold flux systems have been extensively studied in the past few decades,[13–17] only a few investigations regarding the crystallization kinetics and/or mechanism of mold fluxes have been conducted so far.[18–21] Watanabe *et al.*[18] studied the non-isothermal crystallization kinetics of lime-silica-based mold fluxes, and their findings showed that the addition of alkali oxides (Li_2O, Na_2O or K_2O) lowered the activation energy for the mold flux crystallization. Zhou *et al.*[19] reported that the

CHENG-BIN SHI, Formerly Postdoctoral Fellow with the Department of Materials Science and Engineering, Pohang University of Science and Technology (POSTECH), Pohang 790-784, Republic of Korea, is now Assistant Professor with the State Key Laboratory of Advanced Metallurgy, University of Science and Technology Beijing (USTB), Beijing 100083, P.R. China. MYUNG-DUK SEO, Ph.D. Candidate, and SEON-HYO KIM, Professor, are with the Department of Materials Science and Engineering, Pohang University of Science and Technology (POSTECH). HUI WANG, Formerly Visiting Researcher with the Department of Materials Science and Engineering, Pohang University of Science and Technology (POSTECH), is now Assistant Researcher with the Shougang Research Institute of Technology, Beijing 100041, P.R. China. JUNG-WOOK CHO, Research Associate Professor, is with the Graduate Institute of Ferrous Technology, Pohang University of Science and Technology (POSTECH), Pohang 790-784, Republic of Korea. Contact e-mail: jungwook@postech.ac.kr
Manuscript submitted April 27, 2014.
Article published online September 13, 2014.

activation energy for the isothermal crystallization of lime-silica-based mold fluxes decreased with increasing the basicity (mass pctCaO/mass pctSiO_2). Li *et al.*[20] examined the effect of Na_2O addition on the isothermal crystallization kinetics of lime-silica-based mold fluxes based on *in situ* observation technique and revealed that the crystallization activation energy of the studied mold fluxes decreased with increasing Na_2O content. Wang *et al.*[21] investigated the kinetics of non-isothermal crystallization of lime-silica-based mold fluxes with various TiO_2 contents that occurred on heating and found that TiO_2 substitution of SiO_2 in the mold fluxes retarded the crystallization of cuspidine by increasing the activation energy for crystal growth. However, to the best of the authors' knowledge, no investigations have been carried out to reveal the non-isothermal crystallization kinetics of lime-alumina-based mold fluxes.

It has been demonstrated in the authors' most recent studies[22,23] that (I) the newly developed lime-alumina-based mold fluxes are promising substitutes for conventional lime-silica-based systems for continuous casting of high-Al steels, in terms of the heat transfer and lubrication in practical high-Al steels casting as well as the cast slabs quality, (II) the primary crystalline phase in these mold fluxes is cuspidine ($3CaO{\cdot}2SiO_2{\cdot}CaF_2$). In conventional lime-silica-based mold fluxes, cuspidine is also the primary crystalline phase precipitated in mold flux film during continuous casting process.[1,18] It is cuspidine as the primary crystalline phase in conventional lime-silica-based mold fluxes that plays a key role in controlling the horizontal heat transfer between solidifying steel shell and mold in continuous casting.[18,24]

In consideration of the great practical significance, the present investigation was undertaken to extend the previous studies[22,23] on the development of lime-alumina-based mold fluxes to reveal the crystallization kinetics and mechanism of the primary crystalline phases in the newly developed mold fluxes. The kinetic parameters (*i.e.*, Avrami exponent and effective activation energy) of lime-alumina-based mold fluxes during non-isothermal crystallization were determined on the basis of differential scanning calorimetry (DSC) results. Furthermore, the crystallization mechanism of the developed mold fluxes was identified based on the obtained kinetic parameters.

II. EXPERIMENTAL

The non-isothermal DSC (Netzsch STA 449C; Netzsch Instrument Inc., Germany) measurements were performed to study the crystallization kinetics of the newly developed lime-alumina-based mold fluxes New2, New3, New4, New5, and New6. The chemical compositions of the studied mold fluxes are listed in Table I. For each DSC experiment, approximately 60 mg of sample powders was heated at a constant heating rate of 20 K/min from room temperature to 1573 K (1300 °C) in a platinum crucible with a diameter of 5 mm and a height of 5 mm, and then held for 3 minutes to eliminate bubbles and homogenize its chemical composition. Subsequently, the liquid sample was cooled at a constant cooling rate to room temperature. The non-isothermal DSC measurements at the continuous cooling rates of 5, 10, 15, and 20 K/min have been carried out for these mold fluxes in the authors' previous study.[23] To obtain thermal analysis data of the DSC measurements for determining reliable crystallization kinetic parameters of mold flux, supplementary DSC measurements at the continuous cooling rates of 12.5 and/or 17.5 K/min were performed for the studied mold fluxes in the current work.

III. RESULTS AND DISCUSSION

Among the newly developed lime-alumina-based mold fluxes, mold fluxes New4, New5, and New6 show comparatively improved in-mold performance and slab surface quality in casting trials of high-Al transformation-induced plasticity (TRIP) steel.[22,23] The primary crystalline phase in these mold fluxes was confirmed by DSC, XRD, and FE-SEM/EDS determination to be cuspidine ($3CaO{\cdot}2SiO_2{\cdot}CaF_2$).[23] In the lime-alumina-based mold flux with lower B_2O_3 content (5.4 mass pct) and a CaO/Al_2O_3 ratio of 1.2, the primary crystalline phase is CaF_2. In the B_2O_3-free lime-alumina-based mold flux, it is not possible to distinguish the primary crystalline phase between CaF_2 and $3CaO{\cdot}2SiO_2$. The detailed discussion has been given elsewhere.[23] The crystallization kinetics of the primary crystalline phases in the lime-alumina-based mold fluxes was studied and compared with that in the conventional lime-silica-based mold fluxes.

As a kinetic parameter for characterizing the nucleation mode and dimensionality of crystal growth, Avrami exponent for non-isothermal mold flux crystallization was determined by Ozawa equation as well as the combined Avrami–Ozawa method. Moreover, the FE-SEM observations for the studied mold fluxes were employed to verify the crystallization kinetic analysis results. The effective activation energy for non-isothermal crystallization of the newly developed lime-alumina-based mold fluxes was determined as a function of the relative degree of crystallinity using the differential isoconversional method of Friedman.

A. *Ozawa Analysis of Mold Flux Non-isothermal Crystallization*

The isothermal crystallization kinetics is usually described in terms of Avrami equation[25–27]

$$\alpha = 1 - \exp[-(kt)^{n_A}], \qquad [1]$$

where α is the relative degree of crystallinity at a given time t, n_A is the Avrami exponent that is associated with the crystallization mechanism, and k is the effective overall rate constant.

Taking twice the logarithm of Eq. [1] gives the following expression:

$$\ln[-\ln(1-\alpha)] = n_A \ln t + n_A \ln k. \qquad [2]$$

Table I. Chemical Compositions of the Studied Mold Fluxes in the Present Work

Sample No.	Chemical Composition (mass pct)							Viscosity (Pa·s) [1573 K (1300 °C)]	Mass pctCaO/ mass pctAl_2O_3
	CaO	SiO_2	Al_2O_3	Na_2O	F	B_2O_3	Li_2O		
New2	30.7	2.2	25.1	12.3	15.1	5.4	3.1	0.075	1.2
New3	32.0	2.3	26.2	7.4	13.9	–	6.4	0.077	1.2
New4	37.9	9.0	11.4	9.0	8.9	16.0	4.9	0.055	3.3
New5	42.6	11.9	13.0	4.8	9.3	10.8	4.9	0.084	3.3
New6	37.8	8.9	11.5	1.0	8.1	15.0	6.2	0.038	3.3

The relative degree of crystallinity α at any time t can be calculated using the following equation

$$\alpha = \frac{\int_{t_0}^{t_i} (dH_c/dt)dt}{\int_{t_0}^{t_f} (dH_c/dt)dt}, \quad [3]$$

where dH_c is the measured enthalpy of crystallization during an infinitesimal time interval dt in DSC measurement, t_i is the elapsed time during crystallization, t_0 is the time at which the crystallization just begins, and t_f is the time at which the crystallization is completed.

Avrami exponent is generally used as an effective kinetic parameter to characterize the nucleation mode and dimensionality of crystal growth for crystallization. To identify the mechanism of non-isothermal crystallization quantitatively, Ozawa[28] extended Avrami equation from isothermal crystallization to non-isothermal crystallization and derived the following equation for determining Avrami exponent for non-isothermal crystallization based on the mathematical derivation of Evans[29]

$$\ln[-\ln(1-x)] = \ln K(T) - n_O \ln \beta, \quad [4]$$

where x is the relative degree of crystallinity at a given temperature T, β is the cooling rate, $K(T)$ is a function related to the overall crystallization rate, and n_O is the Avrami exponent involved in Ozawa equation for describing non-isothermal crystallization. When Ozawa equation can adequately describe the non-isothermal crystallization behavior, a plot of $\ln[-\ln(1-x)]$ *vs* $\ln \beta$ at a given temperature should give a straight line and its slope yields the value of n_O. The Ozawa equation Eq. [4] has been extensively employed to determine the Avrami exponent for non-isothermal crystallization.[30–33]

The relative degree of crystallinity x at a given temperature T can be calculated from DSC curve with respect to temperature using the following equation

$$x = \frac{\int_{T_0}^{T_i} (dH_c/dT)dT}{\int_{T_0}^{T_f} (dH_c/dT)dT}, \quad [5]$$

where dH_c is the measured enthalpy of crystallization during an infinitesimal temperature interval dT in DSC measurement, T_i is the crystallization temperature at certain time t, T_0 is the temperature at which the crystallization just begins, and T_f is the temperature at which the crystallization is completed.

According to Ozawa method, the double logarithm of relative degree of crystallinity x obtained for various cooling rates at the same crystallization temperature in the temperature intersection range of various cooling rates is plotted against the logarithm of cooling rates to determine the value of Avrami exponent. Figure 1 shows the plots of $\ln[-\ln(1-x)]$ *vs* $\ln \beta$ at specific temperatures for the primary crystalline phase formation in mold fluxes New3, New4, New5, and New6. Since there is no temperature intersection range between the cooling rate of 5 K/min for mold fluxes New4, New5, and New6, 20 K/min for New6 and other cooling rates, the values of relative crystallinity degree x corresponding to these cooling rates at the same crystallization temperatures are unavailable. It is clear from Figure 1 that the Ozawa plots show significant deviation from linearity. Instead, large curvature can be observed in these plots. These results indicate the failure of Ozawa equation in describing the non-isothermal crystallization behavior of the lime-alumina-based mold fluxes.

Figure 2 presents the variation of the relative degree of crystallinity x as a function of cooling rate at the given crystallization temperatures in the temperature intersection range of various cooling rates, which have been used to determine the Avrami exponent as shown in Figure 1. It was observed from Figure 2 that the relative degree of crystallinity x varied in a large range with cooling rate at the same crystallization temperature for the studied crystalline phase in mold fluxes. The results shown in Figure 2 indicate that, under the condition of a given crystallization temperature but different cooling rates, the lower cooling rate corresponds to the point of the crystallization later stage (even the final stage), on the contrary, it is just at the crystallization primary stage (even the initial stage) for the higher cooling rate.

Crystallization consists of both nucleation and crystal growth processes. These processes are strongly dependent on temperature. The nucleation rate and crystal growth rate as a function of temperature are schematically shown in Figure 3. When crystallization commences from a high temperature, the nucleation rate initially increases and then decreases with the decrease in temperature. The nucleation rate reaches maximum at a certain temperature. The crystal growth rate proceeds in a similar way. At the later stage of crystallization, both nucleation and crystal growth are retarded since they take place in a constrained environment.[34] In the overall crystallization process, under the condition of coupled effects of nucleation rate and crystal growth rate,

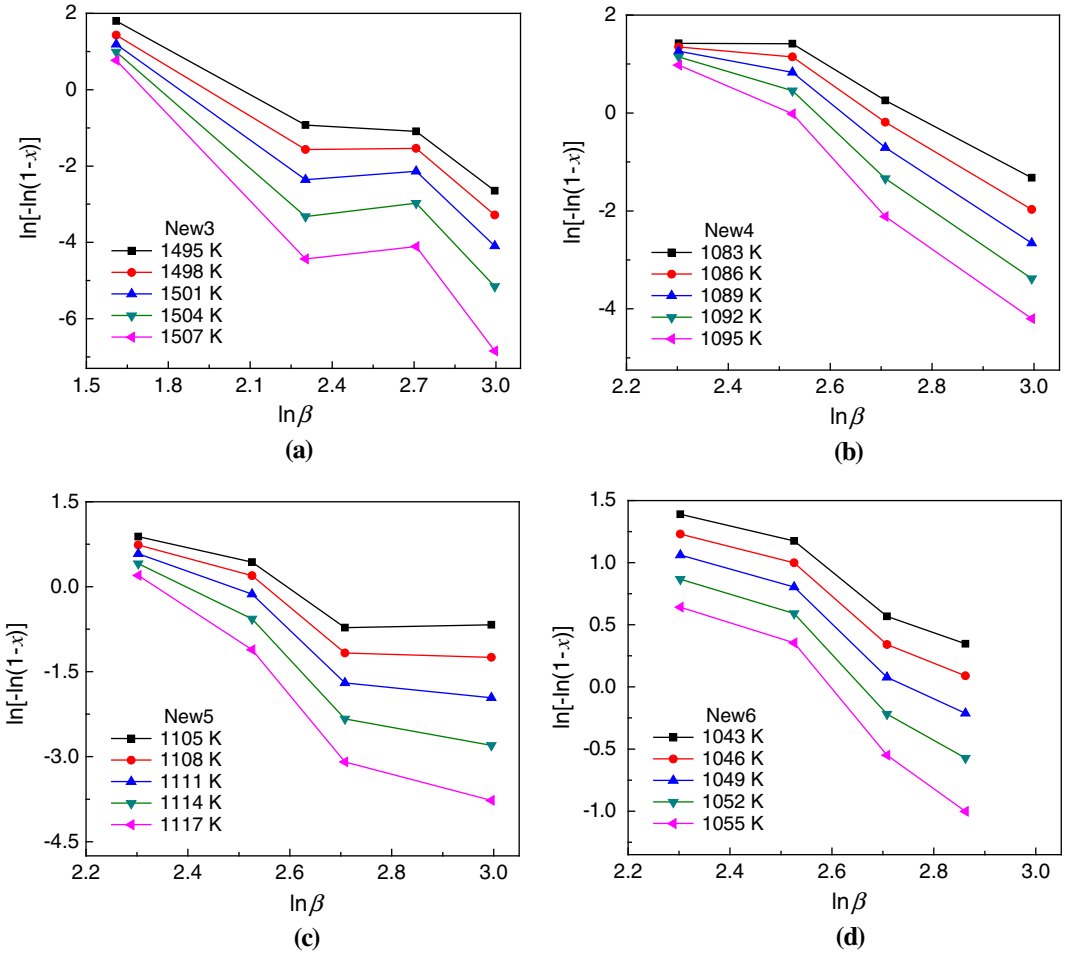

Fig. 1—Plots of $\ln[-\ln(1-x)]$ *vs* $\ln\beta$ for non-isothermal crystallization of mold fluxes: (*a*) New3, (*b*) New4, (*c*) New5, and (*d*) New6.

the crystallization rate is not a constant. As shown in Figure 2, it is just at the initial stage of crystallization at the cooling rates of 20 K/min at these temperatures and 15 K/min at the higher temperatures. On the contrary, the crystallization at the cooling rate of 5 K/min for New3, 10 and 12.5 K/min for New4, New5, and New6 is at the nearly final stage of crystallization at various temperatures. The relative degree of crystallinity x chosen at a given crystallization temperature includes both the values corresponding to the initial stage and the values from the final stage of crystallization due to the variation of the cooling rates. Consequently, the obtained values of the relative degree of crystallinity x with a considerable difference for various cooling rates were employed to construct the Ozawa plot of $\ln[-\ln(1-x)]$ *vs* $\ln\beta$ for non-isothermal crystallization.

However, compared with the primary stage of crystallization, the later stage could be associated with the variation in the chemistry of remaining liquid matrix as successive foregoing crystal formation, the saturation of nucleation sites, and/or mutual contact of crystals. Nevertheless, these factors were not taken into account in the Ozawa method. These should be responsible for the failure of Ozawa method in determining reliable Avrami exponent for the non-isothermal crystallization of mold fluxes New3, New4, New5, and New6, as shown in Figure 1. The present finding demonstrated that the Ozawa method was inapplicable in describing the non-isothermal crystallization mode for the case where there was a significant difference in the relative degree of crystallinity at specific temperatures for various cooling rates, considering the change in crystallization mechanism during successive crystallization. The further discussion will be given later. The failure of Ozawa method in determining Avrami exponent for non-isothermal crystallization was also reported by other researchers.[35–38]

B. *Combined Ozawa–Avrami Analysis of Mold Flux Non-isothermal Crystallization*

Considering that the non-isothermal crystallization of the studied system was not fitted to the Ozawa equation probably due to the inaccurate assumption in the Ozawa theory such as secondary crystallization, dependence of lamellar thickness on crystallization temperature, and the constant cooling function in the overall crystallization process, Mo[38] derived the following equation to describe non-isothermal crystallization by combining the Avrami equation and Ozawa equation.

$$\ln\beta = \ln F(T) - b\ln t, \qquad [6]$$

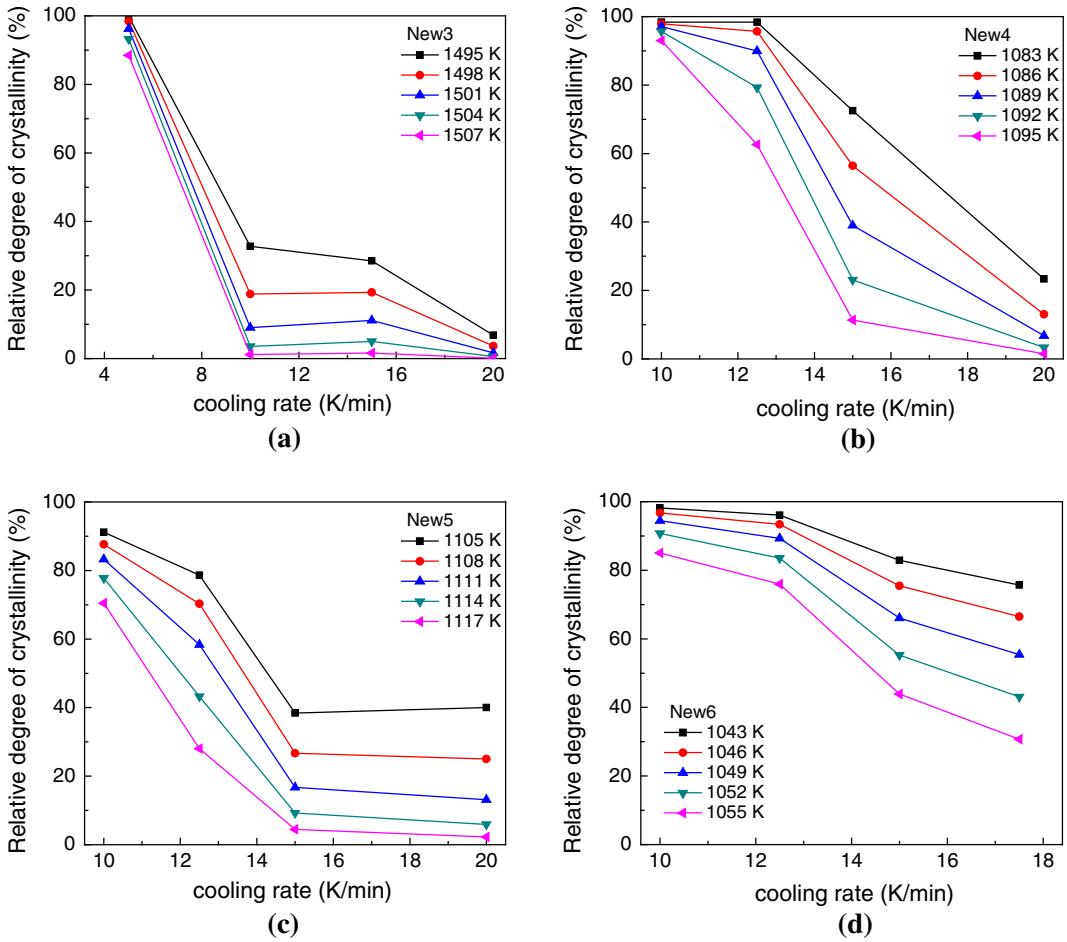

Fig. 2—Relative degree of crystallinity x as a function of continuous cooling rate at specified crystallization temperatures: (*a*) New3, (*b*) New4, (*c*) New5, and (*d*) New6.

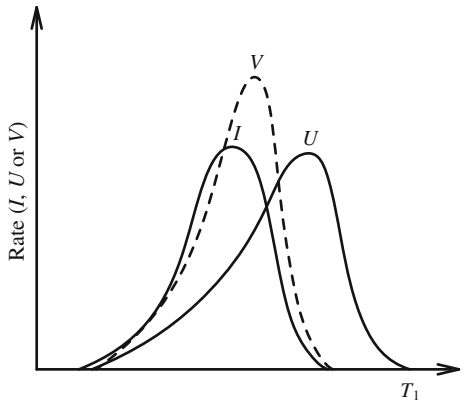

Fig. 3—Schematic diagram of temperature dependence of nucleation rate (I), crystal growth rate (U), and overall crystallization rate (V). T_l denotes liquidus temperature.

where b is the ratio of Avrami exponent n_A to Avrami exponent n_O, $F(T) = [K(T)/k]^{1/n_O}$ refers to the value of cooling rate that must be selected within a unit of crystallization time when the measured systems reach a certain degree of crystallinity. Herein, the non-isothermal crystallization kinetic parameter n_O holds an identical physical meaning with Avrami exponent n_A for isothermal crystallization.[38,39] According to Eq. [6], at a given relative degree of crystallinity, a plot of $\ln \beta$ *vs* $\ln t$ should yield a straight line. The kinetic parameter b can be determined from the slope of the fitted straight line. Based on the determined kinetic parameter b and Avrami exponent estimated by Avrami equation for non-isothermal crystallization (taken as apparent Avrami exponent) as well as the relationship $b = n_A/n_O$, the Avrami exponent n_O with definite physical meaning for non-isothermal crystallization can be obtained.[38,39]

In consideration of the failure of Ozawa method in determining Avrami exponent for describing the non-isothermal crystallization mode of mold fluxes, the combined Avrami–Ozawa method was employed in the current study. Figure 4 shows the plots of $\ln \beta$ *vs* $\ln t$ at various relative degrees of crystallinity. It is clear from Figure 4 that all plots show good linear relationship between $\ln \beta$ and $\ln t$, verifying the applicability of the combined Avrami and Ozawa equation in describing the non-isothermal crystallization of mold fluxes. The estimated values of kinetic parameter b from the slopes of linear-fitted lines are summarized in Table II. It is noted that the values of b at different relative degrees of crystallinity are almost constant for each mold flux.

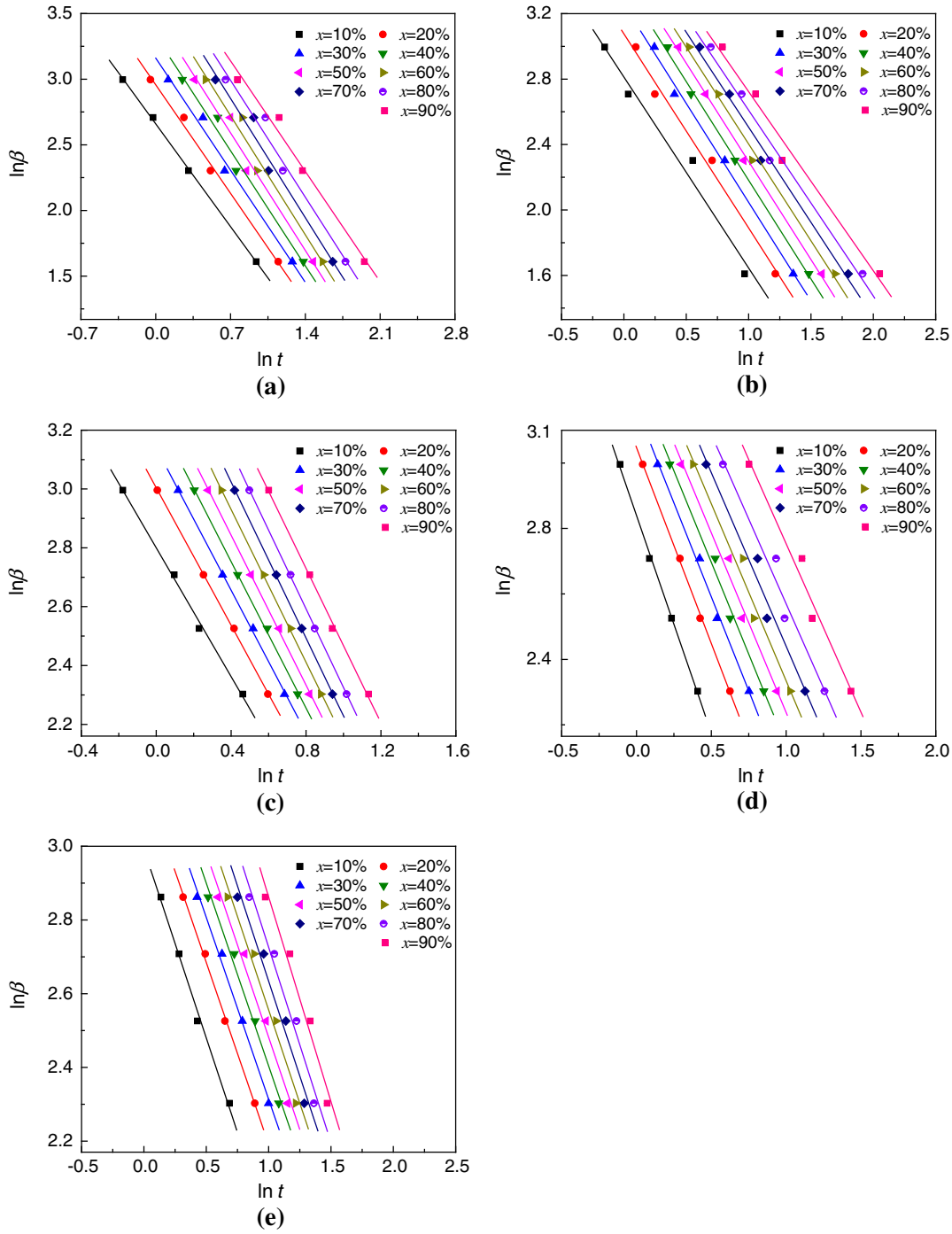

Fig. 4—Plots of ln β *vs* ln t for non-isothermal crystallization of mold fluxes at various relative degrees of crystallinity x: (*a*) New2, (*b*) New3, (*c*) New4, (*d*) New5, and (*e*) New6.

According to Avrami equation, the Avrami plots of $\ln[-\ln(1-x)]$ *vs* ln t for non-isothermal crystallization of mold fluxes at various cooling rates are presented in Figure 5. It can be seen that the plots can be divided into two linear sections along with ln t, which are designated as the primary stage and the secondary stage of crystallization, respectively, except a single linearity for mold flux New3. The primary stage of crystallization shows good linear relationship. At the secondary stage (*i.e.*, the upper part of the plot), the plots tend to deviate from the linearity of the crystallization primary stage, and exhibit another linear relationship. The deviation of the Avrami plot at the later stage of non-isothermal crystallization was also observed in other studies.[37–39] The deviation of the Avrami plot at the later stage is attributed to the fact that the non-isothermal crystallization at this stage could be associated with the variation in the chemistry of remaining liquid matrix as successive foregoing crystal formation, the saturation of nucleation sites, and/or mutual contact of crystals, as

discussed in Section III–A. The present results suggest a change in the crystallization mechanism of CaF_2 in mold flux New2, cuspidine in mold fluxes New4, New5, and New6 between the primary stage and the secondary stage of crystallization.

It should be noted that the Avrami exponent n_A for non-isothermal crystallization does not have the same physical significance as that in isothermal crystallization because the temperature changes constantly during non-isothermal crystallization. For non-isothermal crystallization, n_A is designated as the apparent Avrami exponent.[38,39] The values of apparent Avrami exponent n_A can be estimated from the slopes of linear fitted straight lines, respectively, for the primary stage and the secondary stage of crystallization shown in Figure 5. As shown in Figure 5, the linearity of fitted straight lines are relatively parallel for different cooling rates at the same crystallization stage (*i.e.*, primary stage or secondary stage), indicating that the apparent Avrami exponent for mold flux non-isothermal crystallization does not change significantly with the cooling rate, except for only a few cases. The values of apparent Avrami exponent n_A for the primary stage and the secondary stage of crystallization of the studied mold fluxes are summarized in Table III.

To describe the non-isothermal crystallization mode of mold fluxes, the Avrami exponent for non-isothermal crystallization n_O was estimated from the obtained values of b and apparent Avrami exponent n_A, according to the combined Avrami–Ozawa method, as well as the relationship $b = n_A/n_O$. The calculated values of Avrami exponent n_O corresponding to various relative degrees of crystallinity are listed in Table IV.

The Avrami exponent n_O for non-isothermal crystallization of CaF_2 in mold flux New2 was determined to be close to 2.5 at the crystallization primary stage (the relative degree of crystallinity smaller than 60 pct), and approach to 2.0 at the later stage, as shown in Table IV. Considering the present case where the non-isothermal mold flux melt crystallization did not occur with a constant number of nuclei, the estimated values of Avrami exponent suggested that the crystallization of CaF_2 occurred through bulk nucleation and diffusion-controlled three-dimensional growth, and then transformed to diffusion-controlled two-dimensional growth at the crystallization later stage. The microstructure observation of mold flux New2 by FE-SEM provided further evidence for the current finding (see Figure 7 in Reference 23). It is found that the Avrami exponent for the first crystalline phase formation in mold flux New3 is close to 3.0 in the overall crystallization process, which is an indication of a bulk nucleation and reaction-controlled two-dimensional growth.

For the crystallization of cuspidine in mold flux New4, the values of Avrami exponent were determined to be close to 4.0 at the crystallization primary stage, and approach to 3.0 at the later stage. This result indicates that at the primary stage of cuspidine crystallization, bulk nucleation and reaction-controlled three-dimensional growth take place, and then the crystallization transforms to reaction-controlled two-dimensional growth at the later stage. The same crystallization mode was observed for the non-isothermal crystallization of cuspidine in mold flux New6 based on the obtained Avrami exponent values shown in Table IV. The FE-SEM observations show that the morphology of individual cuspidine in mold fluxes New4 and New6 is faceted (see Figures 9 and 11 in Reference 23), which supports the current finding of kinetic analysis.

For the lime-alumina-based mold flux with lower B_2O_3 content (10.8 mass pct), the values of Avrami exponent for the non-isothermal crystallization of cuspidine were determined as 2.85 to 3.50 for the primary stage (the relative degree of crystallinity smaller than 70 pct) and 2.02 to 2.08 for the later stage. It suggests that the crystallization of cuspidine occurs through bulk nucleation and reaction-controlled two-dimensional growth followed by reaction-controlled one-dimensional growth at the crystallization later stage, or bulk nucleation and reaction-controlled two-dimensional growth followed by diffusion-controlled two-dimensional growth at the crystallization later stage. However, combining the observed morphology of cuspidine in mold flux New5 by FE-SEM (see Figure 10 in Reference 23) with the obtained Avrami exponent values, it can be deduced that the crystallization of cuspidine in mold flux New5 is bulk nucleation and reaction-controlled two-dimensional growth at the crystallization primary stage, which then transforms to diffusion-controlled two-dimensional growth.

Table II. Values of Kinetic Parameter *b* at Various Relative Degrees of Crystallinity *x* Determined Using the Combined Avrami–Ozawa Equation

Sample No.	Crystalline Phase	Kinetic Parameter b								
		x = 10 pct	x = 20 pct	x = 30 pct	x = 40 pct	x = 50 pct	x = 60 pct	x = 70 pct	x = 80 pct	x = 90 pct
New2	CaF_2	1.12	1.18	1.22	1.25	1.27	1.29	1.29	1.27	1.20
New3	—*	1.17	1.18	1.21	1.21	1.20	1.18	1.16	1.14	1.10
New4	$3CaO{\cdot}2SiO_2{\cdot}CaF_2$	1.10	1.17	1.21	1.24	1.27	1.30	1.33	1.34	1.31
New5	$3CaO{\cdot}2SiO_2{\cdot}CaF_2$	1.33	1.20	1.15	1.20	1.10	1.08	1.06	1.03	1.03
New6	$3CaO{\cdot}2SiO_2{\cdot}CaF_2$	1.02	0.99	0.99	0.99	1.00	1.01	1.03	1.06	1.11

*No distinguishable crystalline phase between CaF_2 and $3CaO{\cdot}2SiO_2$ can be confirmed as the first and the second crystalline phase in mold flux New3. The detailed discussion has been given in Reference 23.

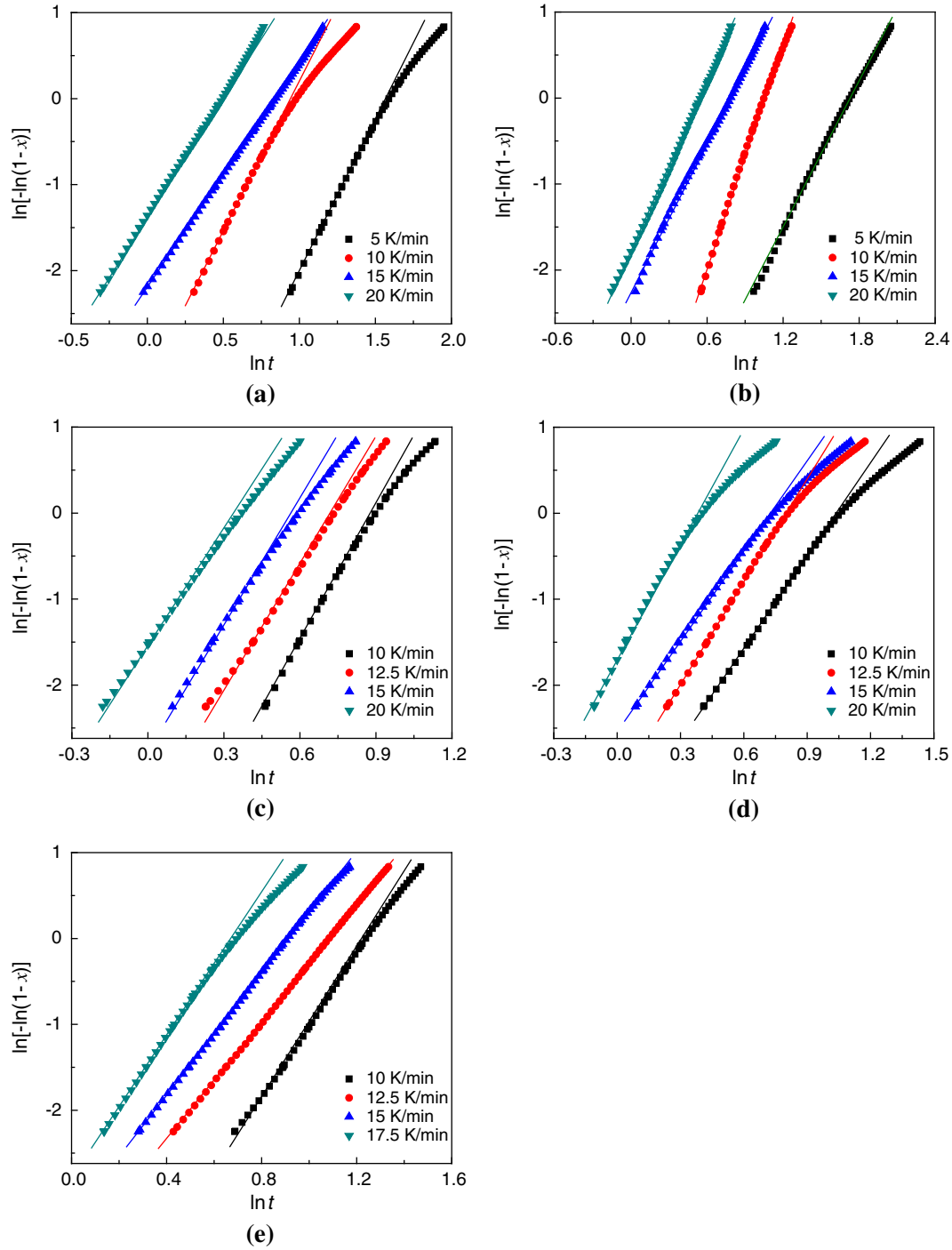

Fig. 5—Plots of $\ln[-\ln(1-x)]$ *vs* $\ln t$ for non-isothermal crystallization of mold fluxes at different cooling rates: (*a*) New2, (*b*) New3, (*c*) New4, (*d*) New5, and (*e*) New6.

The difference in the crystallization mode of cuspidine in mold fluxes New4, New6, and New5 is expected to be due to the fact that the viscosity of mold flux New5 is higher than that of New4 and New6, resulting in a higher diffusion resistance for mold flux components. Consequently, the growth of cuspidine in mold flux New5 (mass pctCaO/mass pctSiO_2 = 3.58) is controlled by diffusion at the crystallization later stage as a result of the further decrease of SiO_2 content after successive formation of cuspidine in the mold flux.

The present findings regarding the crystallization mode of cuspidine in the lime-alumina-based mold fluxes are different from that for lime-silica-based mold fluxes reported by Zhou *et al.*,[19] based on single hot thermocouple technique (SHTT) isothermal crystallization observation and Johnson–Mehl–Avrami (JMA) model, showing that the crystallization of cuspidine in the mold fluxes changed from one-dimensional growth to three-dimensional growth with a constant number of nuclei when the basicity of mold fluxes increased from

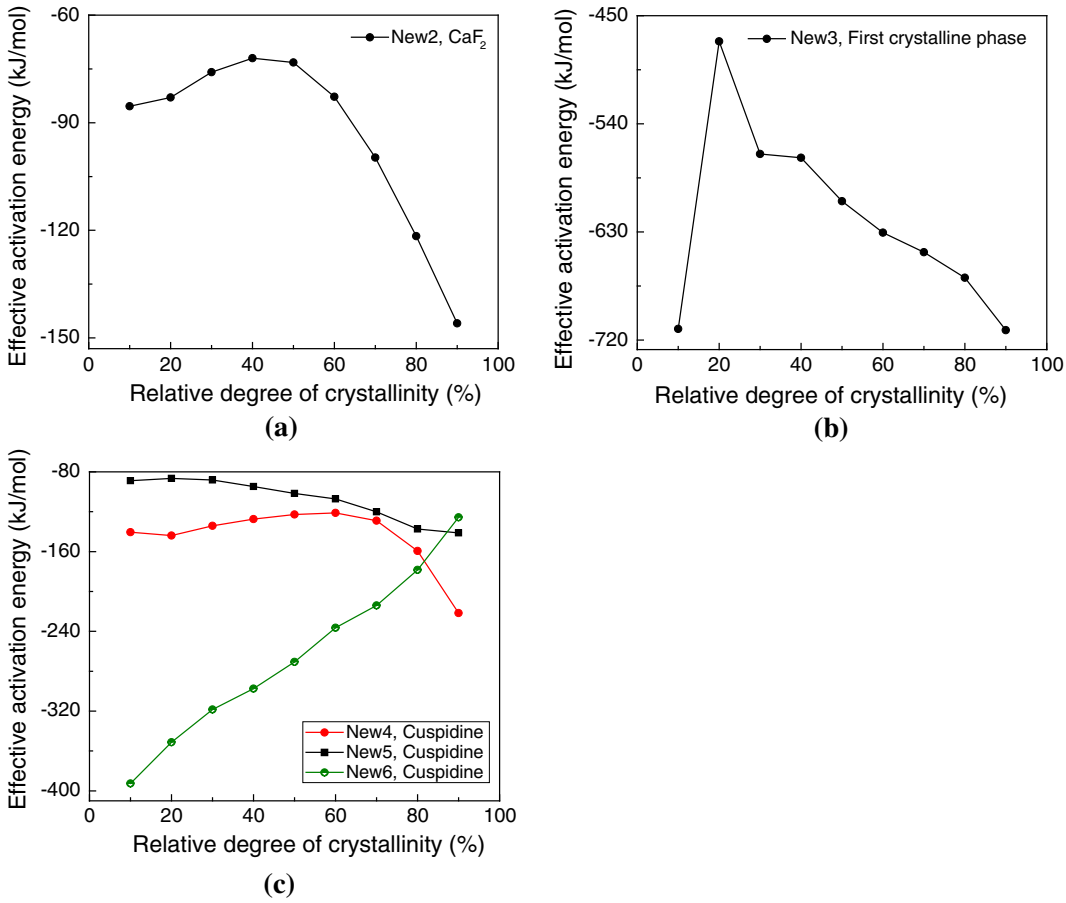

Fig. 6—Dependence of the effective activation energy on the relative degree of crystallinity: (*a*) New2, (*b*) New3, and (*c*) New4, New5, and New6.

0.8 to 1.2, as well as the results reported by Wang *et al.*[21] who noted the surface crystallization of cuspidine during lime-silica-based mold fluxes with varying TiO_2 content (0, 5, and 10 mass pct) crystallization from glassy state. Since only a few studies on the non-isothermal crystallization mode of cuspidine in mold fluxes have been reported, this fact makes it extremely limited to further compare the present results with other findings.

C. *Effective Activation Energies for Non-isothermal Crystallization of Mold Fluxes*

Since the crystallization of mold flux in practical continuous casting process occurs from melt in a cooling process, the kinetics of non-isothermal mold flux crystallization from the melt during cooling process was investigated in the current work. For non-isothermal crystallization kinetic analysis, various models have been developed to estimate the activation energy associated with crystallization from thermal analysis data over the past 60 years, including Kissinger equation,[40] Ozawa equation,[41] modified Ozawa–Chen equation,[42] and Matusita equation.[43,44] Among these models, Kissinger equation[40] and Matusita equation[43] are the most widely used approaches to determine the activation energy for the crystallization that occurs on heating,[30,31,45,46] moreover, they are frequently applied for the non-isothermal crystallization of polymer melts[36–38,47,48] and mold flux[49] that occurs on cooling.

However, it should be stressed that the above-mentioned equations are theoretically only valid to estimate the activation energy associated with the non-isothermal crystallization that occurs on heating, but inapplicable for the melt crystallization that occurs on cooling. To this concern, the differential iso-conversional method developed by Friedman[50] was employed to determine the effective activation energy for mold flux melt crystallization in the present work. Friedman equation[50] has been widely used to evaluate the effective activation energy for non-isothermal melt crystallization that occurs on cooling.[51–53]

The Friedman equation is expressed as

$$\ln\left(\frac{\mathrm{d}x}{\mathrm{d}t}\right)_{x,i} = -\frac{E_x}{RT_{x,i}} + \text{constant}, \qquad [7]$$

where $\frac{\mathrm{d}x}{\mathrm{d}t}$ is the instantaneous crystallization rate as a function of time at a given relative degree of crystallinity x, R is the gas constant, $T_{x,i}$ is the set of absolute temperatures related to a given relative degree of crystallinity at different cooling rates, E_x is the effective activation energy for crystallization at a given relative degree of crystallinity, and the subscript i is the ordinal

Table III. Apparent Avrami Exponent n_A for Non-isothermal Crystallization Determined Using Avrami Method

Sample No.	Crystalline Phase	Cooling Rate (K/min)	Apparent Avrami Exponent (n_A)	
			Crystallization Primary Stage	Crystallization Secondary Stage
New2	CaF_2	5	3.54	2.32
		10	3.48	2.11
		15	2.61	2.66
		20	2.81	3.05
New3	—*	5	2.84	–
		10	4.29	–
		15	2.89	–
		20	3.28	–
New4	$3CaO{\cdot}2SiO_2{\cdot}CaF_2$	10	5.31	3.62
		12.5	4.45	4.10
		15	4.60	3.72
		20	4.17	3.64
New5	$3CaO{\cdot}2SiO_2{\cdot}CaF_2$	10	3.51	2.08
		12.5	3.94	2.12
		15	3.41	2.16
		20	4.31	2.21
New6	$3CaO{\cdot}2SiO_2{\cdot}CaF_2$	10	4.12	3.65
		12.5	3.42	3.35
		15	3.57	3.22
		17.5	4.14	3.03

*Same annotation as detailed in Table II.

Table IV. Values of Avrami Exponent n_O for Non-isothermal Mold Flux Crystallization at Various Relative Degrees of Crystallinity x Determined Using the Combined Avrami–Ozawa Equation

Sample No.	Crystalline Phase	Avrami Exponent n_O at Various Relative Degrees of Crystallinity x								
		x = 10 pct	x = 20 pct	x = 30 pct	x = 40 pct	x = 50 pct	x = 60 pct	x = 70 pct	x = 80 pct	x = 90 pct
New2	CaF_2	2.78	2.63	2.55	2.48	2.43	1.96	1.96	1.99	2.11
New3	—*	2.85	2.80	2.75	2.75	2.77	2.81	2.86	2.93	3.03
New4	$3CaO{\cdot}2SiO_2{\cdot}CaF_2$	4.23	3.96	3.82	3.72	3.64	2.90	2.85	2.82	2.88
New5	$3CaO{\cdot}2SiO_2{\cdot}CaF_2$	2.85	3.16	3.29	3.38	3.45	3.50	2.02	2.07	2.08
New6	$3CaO{\cdot}2SiO_2{\cdot}CaF_2$	3.73	3.86	3.86	3.85	3.81	3.27	3.21	3.12	2.99

*Same annotation as detailed in Table II.

number of individual cooling rate. The instantaneous crystallization rate $\frac{dx}{dt}$ can be determined from DSC data using the following equation

$$\frac{dx}{dt} = \frac{dH_c/dt}{\int_{t_0}^{t_f} (dH_c/dt)dt}. \quad [8]$$

The effective activation energy E_x at different relative degrees of crystallinity x can be calculated from the slope of the linear fitted plot of $\ln(dx/dt)$ *vs* $1/T_x$ from DSC experimental data.

The dependence of the effective activation energy on the relative degree of crystallinity is presented in Figure 6. As shown in Figure 6(c), the effective activation energy for the cuspidine crystallization in mold flux New4 increases with the increase in the relative degree of crystallinity, and then decreases at the relative degree of crystallinity greater than 60 pct. For the crystallization of CaF_2 in mold flux New2, the curve exhibits a similar trend with a transition point at the relative degree of crystallinity x greater than 50 pct, as shown in Figure 6(a). These results reveal that the crystallization of cuspidine in mold flux New4 and CaF_2 in mold flux New2 becomes more difficult, and then gets easier at the relative degree of crystallinity x greater than 60 and 50 pct, respectively. The monotonous decrease in the effective activation energy for the first crystalline phase formation with the increase in the relative degree of crystallinity was observed for mold flux New3, except for x = 10 pct, as shown in Figure 6(b), suggesting that the crystallization got easier as the crystallization progressed.

It was noted that the transition point of these trends approximately corresponded to the relative degree of crystallinity at which the crystallization mode of cuspidine in mold flux New4 and CaF_2 in mold flux New2

transformed. However, a similar trend of the dependence of effective activation energy on the relative degree of crystallinity was not observed for the crystallization of cuspidine in mold fluxes New5 and New6, even the crystallization mode of cuspidine changed in these mold fluxes during the overall crystallization process.

For the crystallization of cuspidine in mold flux New5, the effective activation energy decreases monotonically from −88.81 kJ/mol at $x = 10$ pct to −141.19 kJ/mol at $x = 90$ pct. It indicates that the crystallization of cuspidine in mold flux New5 gets easier as the crystallization progresses. It was observed from Figure 6(c) that the effective activation energy for cuspidine crystallization in mold flux New6 increased linearly with the increase in the relative degree of crystallinity, suggesting that it was more difficult for cuspidine to crystallize as the crystallization proceeded. The effective activation energy for cuspidine formation in the mold flux New5 during the whole crystallization process is higher than that for cuspidine formation in mold fluxes New4 and New6 as shown in Figure 6(c). This could be due to the fact that the viscosity of mold flux New5 is much higher than that of mold fluxes New4 and New6 as listed in Table I, which results in the higher transfer resistance of ion clusters in mold flux New5.

The monotonous variation in effective activation energy for mold fluxes New5 and New6 is attributed to the increase in B_2O_3 and Na_2O contents in remaining liquid matrix as successive foregoing crystallization of cuspidine ($3CaO{\cdot}2SiO_2{\cdot}CaF_2$) proceeds in mold fluxes New5 and New6. B_2O_3 could act as a network former and enhance glass-formation ability of mold flux, resulting in suppression of cuspidine crystallization ability in the mold flux. On the contrary, Na_2O plays a role as a network modifier in dividing the silicate flow unit in mold fluxes and lowering the melting temperature of mold fluxes,[18] as well as lowering the transfer resistance of ion clusters and energy barrier for crystallization by decreasing viscosity of mold flux,[20] which would enhance mold flux crystallization. Under the condition of coupled effects of continuously increasing B_2O_3 and Na_2O contents in remaining liquid matrix as successive foregoing cuspidine crystallization in the mold flux with lower B_2O_3 (10.8 mass pct) and higher Na_2O contents (4.8 mass pct), the monotonous decrease in effective activation energy for cuspidine crystallization is attributed to the fact that the enhancement of cuspidine crystallization induced by Na_2O exceeds the suppression of the crystallization ability by B_2O_3. Since the mold flux New6 contains higher B_2O_3 (15.0 mass pct) and lower Na_2O contents (1.0 mass pct), the reason for the increase in effective activation energy for cuspidine crystallization in the mold flux is just the opposite, compared with mold flux New5.

IV. CONCLUSIONS

The non-isothermal crystallization kinetics of the newly developed lime-alumina-based mold fluxes was investigated by DSC in terms of the Avrami exponent and effective activation energy for crystallization. The conclusions are summarized as follows:

1. Ozawa method fails to describe the non-isothermal crystallization mode of mold fluxes for the case where there is a considerable difference in the relative degree of crystallinity at specific temperatures for various cooling rates, whereas the combined Avrami–Ozawa equation can successfully describe the non-isothermal crystallization mode of the mold fluxes.
2. The crystallization of cuspidine in lime-alumina-based mold fluxes with higher B_2O_3 content occurs through bulk nucleation and reaction-controlled three-dimensional growth, and then transforms to reaction-controlled two-dimensional growth at the crystallization later stage; whereas in the mold fluxes with lower B_2O_3 content (10.8 mass pct), the crystallization of cuspidine is a bulk nucleation and reaction-controlled two-dimensional growth at the crystallization primary stage followed by diffusion-controlled two-dimensional growth process. The crystallization of CaF_2 in mold flux originates from bulk nucleation and diffusion-controlled three-dimensional growth, which then transforms to two-dimensional growth. These kinetic analysis results were confirmed by FE-SEM observations.
3. The effective activation energy for cuspidine crystallization in the mold flux with 16.0 mass pct B_2O_3 and 9.0 mass pct Na_2O increases as the crystallization progresses, and then decreases at the relative degree of crystallinity greater than 60 pct. The transition point of this trend approximately corresponds to the relative degree of crystallinity at which the crystallization mode of cuspidine transforms. For the mold flux with lower B_2O_3 content (15.0 mass pct) and 1.0 mass pct Na_2O, the effective activation energy for cuspidine formation increases linearly with the increase in the relative degree of crystallinity. The effective activation energy for cuspidine formation in the mold flux with lower B_2O_3 content (10.8 mass pct) and 4.8 mass pct Na_2O decreases monotonically as the crystallization proceeds, which is higher than that for cuspidine formation in mold fluxes New4 and New6.

ACKNOWLEDGMENTS

This work was financially supported by the Global Excellent Technology Innovation (Grant No. 10045029) funded by the Ministry of Trade, Industry & Energy (MOTIE) of Korea.

REFERENCES

1. K.C. Mills, A.B. Fox, Z. Li, and R.P. Thackray: *Ironmak. Steelmak.*, 2005, vol. 32, pp. 26–34.
2. H. Nakada, H. Fukuyama, and K. Nagata: *ISIJ Int.*, 2006, vol. 46, pp. 1660–67.

3. A.B. Fox, K.C. Mills, D. Lever, C. Bezerra, C. Valadares, I. Unamuno, J.J. Laraudogoitia, and J. Gisby: *ISIJ Int*., 2005, vol. 45, pp. 1051–58.
4. J.W. Cho, H. Shibata, T. Emi, and M. Suzuki: *ISIJ Int*., 1998, vol. 38, pp. 440–46.
5. T.J.H. Billany, A.S. Normanton, K.C. Mills, and P. Grieveson: *Ironmak. Steelmak*., 1991, vol. 18, pp. 403–10.
6. J.W. Cho, H. Shibata, T. Emi, and M. Suzuki: *ISIJ Int*., 1998, vol. 38, pp. 268–75.
7. W. Wang and A.W. Cramb: *ISIJ Int*., 2005, vol. 45, pp. 1864–70.
8. W. Wang, K. Gu, L. Zhou, F. Ma, I. Sohn, D.J. Min, H. Matsuura, and F. Tsukihashi: *ISIJ Int*., 2011, vol. 51, pp. 1838–45.
9. J.W. Cho, T. Emi, H. Shibata, and M. Suzuki: *ISIJ Int*., 1998, vol. 38, pp. 834–42.
10. T. Kajitani, K. Okazawa, W. Yamada, and H. Yamamura: *ISIJ Int*., 2006, vol. 46, pp. 250–56.
11. M. Hayashi, R.A. Abas, and S. Seetharaman: *ISIJ Int*., 2004, vol. 44, pp. 691–97.
12. H. Nakada, M. Susa, Y. Seko, M. Hayashi, and K. Nagata: *ISIJ Int*., 2008, vol. 48, pp. 446–53.
13. Y. Kashiwaya, C.E. Cicutti, and A.W. Cramb: *ISIJ Int*., 1998, vol. 38, pp. 357–65.
14. W. Wang, K. Blazek, and A. Cramb: *Metall. Mater. Trans. B*, 2008, vol. 39B, pp. 66–74.
15. H.G. Ryu, Z.T. Zhang, J.W. Cho, G.H. Wen, and S. Sridhar: *ISIJ Int*., 2010, vol. 50, pp. 1142–50.
16. L. Zhou, W. Wang, D. Huang, J. Wei, and J. Li: *Metall. Mater. Trans. B*, 2012, vol. 43B, pp. 925–36.
17. M. Hanao: *ISIJ Int*., 2013, vol. 53, pp. 648–54.
18. T. Watanabe, H. Hashimoto, M. Hayashi, and K. Nagata: *ISIJ Int*., 2008, vol. 48, pp. 925–33.
19. L. Zhou, W. Wang, F. Ma, J. Li, J. Wei, H. Matsuura, and F. Tsukihashi: *Metall. Mater. Trans. B*, 2012, vol. 43B, pp. 354–62.
20. J. Li, W. Wang, J. Wei, D. Huang, and H. Matsuura: *ISIJ Int*., 2012, vol. 52, pp. 2220–25.
21. Z. Wang, Q. Shu, and K. Chou: *Metall. Mater. Trans. B*, 2013, vol. 44B, pp. 606–13.
22. J.W. Cho, K. Blazek, M. Frazee, H.B. Yin, J.H. Park, and S.W. Moon: *ISIJ Int*., 2013, vol. 53, pp. 62–70.
23. C.B. Shi, M.D. Seo, J.W. Cho, and S.H. Kim: *Metall. Mater. Trans. B*, 2014, vol. 45B, pp. 1081–97.
24. H. Nakada and K. Nagata: *ISIJ Int*., 2006, vol. 46, pp. 441–49.
25. M. Avrami: *J. Chem. Phys*., 1939, vol. 7, pp. 1103–12.
26. M. Avrami: *J. Chem. Phys*., 1940, vol. 8, pp. 212–24.
27. M. Avrami: *J. Chem. Phys*., 1941, vol. 9, pp. 177–84.
28. T. Ozawa: *Polymer*, 1971, vol. 12, pp. 150–58.
29. U.R. Evans: *Trans. Faraday Soc*., 1945, vol. 41, pp. 365–74.
30. C.T. Cheng, M. Lanaganw, B. Jones, J.T. Lin, and M.J. Pan: *J. Am. Ceram. Soc*., 2005, vol. 88, pp. 3037–42.
31. B. Rangarajan, T. Shrout, and M. Lanagan: *J. Am. Ceram. Soc*., 2009, vol. 92, pp. 2642–47.
32. A. Karamanov, I. Avramov, L. Arrizza, R. Pascova, and I. Gutzow: *J. Non-Cryst. Solids*, 2012, vol. 358, pp. 1486–90.
33. J.M. Pérez, R. Casasola, J.M. Rincón, and M. Romero: *J. Non-Cryst. Solids*, 2012, vol. 358, pp. 2741–48.
34. W. Höland and G.H. Beall: *Glass-Ceramic Technology*, 2nd ed., Wiley, Hoboken, NJ, 2012, pp. 40–74.
35. Y. Tao, Y. Pan, Z. Zhang, and K. Mai: *Eur. Polym. J*., 2008, vol. 44, pp. 1165–74.
36. M. Joshi and B.S. Butola: *Polymer*, 2004, vol. 45, pp. 4953–68.
37. S.H. Kim, S.H. Ahn, and T. Hirai: *Polymer*, 2003, vol. 44, pp. 5625–34.
38. T. Liu, Z. Mo, S. Wang, and H. Zhang: *Polym. Eng. Sci*., 1997, vol. 37, pp. 568–75.
39. Z. Mo: *Acta Polym. Sin*., 2008, vol. 7, pp. 656–61.
40. H.E. Kissinger: *Anal. Chem*., 1957, vol. 29, pp. 1702–06.
41. T. Ozawa: *J. Therm. Anal*., 1970, vol. 2, pp. 301–24.
42. H.S. Chen: *J. Non-Cryst. Solids*, 1978, vol. 27, pp. 257–63.
43. K. Matusita and S. Sakka: *J. Non-Cryst. Solids*, 1980, vols. 38–39, pp. 741–46.
44. K. Matusita, T. Komatsu, and R. Yokota: *J. Mater. Sci*., 1984, vol. 19, pp. 291–96.
45. S.R. Teixeiraw, M. Romero, and J.M. Rincón: *J. Am. Ceram. Soc*., 2010, vol. 93, pp. 450–55.
46. M. Romero, J. Martíın-Márquez, and J.M. Rincón: *J. Eur. Ceram. Soc*., 2006, vol. 26, pp. 1647–52.
47. K.Y. Mya, K.P. Pramoda, and C.B. He: *Polymer*, 2006, vol. 47, pp. 5035–43.
48. S. Zhao, Z. Cai, and Z. Xin: *Polymer*, 2008, vol. 49, pp. 2745–54.
49. S.Y. Choi, D.H. Lee, D.W. Shin, S.Y. Choi, J.W. Cho, and J.M. Park: *J. Non-Cryst. Solids*, 2004, vols. 345–346, pp. 157–60.
50. H.L. Friedman: *J. Polym. Sci. C*, 1964, vol. 6, pp. 183–95.
51. G.Z. Papageorgioua, D.S. Achiliasa, S. Nanakia, T. Beslikasb, and D. Bikiaris: *Thermochim. Acta*, 2010, vol. 511, pp. 129–39.
52. H. Liang, F. Xie, F. Guo, B. Chen, F. Luo, and Z. Jin: *Polym. Bull*., 2008, vol. 60, pp. 115–27.
53. N. Apiwanthanakorn, P. Supaphol, and M. Nithitanakul: *Polym. Test*., 2004, vol. 23, pp. 817–26.